INVITED REVIEW — International Conference on Nanoscience & Technology, China 2013

Silicon nanoparticles: Preparation, properties, and applications*

Chang Huan(常 欢)[a)b)] and Sun Shu-Qing(孙树清)[a)†]

[a)] *Shenzhen Key Laboratory for Minimally Invasive Medical Technologies, Graduate School at Shenzhen, Tsinghua University, Shenzhen* 518055, *China*
[b)] *Department of Biomedical Engineering, Tsinghua University, Beijing* 100084, *China*

(Received 4 September 2013; revised manuscript received 14 March 2014; published online 10 June 2014)

Silicon nanoparticles have attracted great attention in the past decades because of their intriguing physical properties, active surface state, distinctive photoluminescence and biocompatibility. In this review, we present some of the recent progress in preparation methodologies and surface functionalization approaches of silicon nanoparticles. Further, their promising applications in the fields of energy and electronic engineering are introduced.

Keywords: silicon, nanoparticle, quantum confinement effect, optical performance

PACS: 81.07.Bc, 62.25.–g, 03.65.Ta, 78.20.–e. **DOI:** 10.1088/1674-1056/23/8/088102

1. Introduction

With the rapid development of nanoscience and nanotechnology in multidisciplinary fields, nanomaterials have attracted extensive attention. Since the discovery of the bright red-orange fluorescence from electrochemically etched nanoporous silicon (Si) (silicon nanoparticle thin film) upon UV excitation in 1990,[1] heavy-metal-free nanoscale silicon has been investigated in depth for its unparalleled physical and chemical properties such as the feasibility for surface functionalization, size-dependent multicolor light emission, stability against photobleaching and intriguingly, favorable nontoxicity which has been reported to be ten times safer than those of cadmium-based counterparts *in vitro*.[2] The comprehensive superiorities open a new avenue to the application of Si nanoparticles (NPs) to energy source, electronic, sensor, catalysis and biomedical purposes.[3–7]

Unlike other semiconductors, silicon is an indirect bandgap material and manifests remarkable changes in optical and electronic properties when its size approximates to the bulk Bohr radius (4 nm for silicon). By increasing the radiative recombination probability through band-gap transitions instead of phonon-assisted indirect band-gap transitions, the intensity of photoluminescence (PL) can be greatly enhanced. Though until now there has been no consensus on the origin of these amazing characteristics of silicon nanocrystals, and many researchers confirm that these particular properties mostly derive from the combination of quantum confinement and surface states.[8,9] To have a comprehensive understanding of size-dependent phenomenon and other excellent properties, the morphologies and dimensions of Si nanocrystals must be well controlled either by synthetic approaches or subsequent analytical size-selected methods.[10] The morphologies and sizes have been successfully regulated particularly in many narrow band gap II–VI, IV–VI, III–V semiconductor nanoparticles[11] especially cadmium selenide (CdSe) quantum dots (QDs). However, enthusiasm for their prevalent use is subject to its potential toxicity.[12] In order to reduce the release of cadmium ion *in vivo*, a zinc sulfide (ZnS) shell is usually an ideal solution since it can not only improve bioavailability but also increase the quantum yield (QY) of cadmium QDs. Unfortunately, residual toxicity is still an insurmountable obstacle especially for biological and medical applications.

Here, we briefly discuss Si NPs, from their basic method of synthesis and special properties to Si nanocrystal-related physical applications. The rest of this paper is organized as follows. In Section 2, we review the progress in the synthesis techniques of Si nanocrystals, which has been made in the last decade, and focus our attention on the key synthetic processes and developments that have been achieved. In Section 3, we pay close attention to the outstanding PL and electrical characteristics which pave the way to special functional applications different from those of the bulk counterpart. Finally, by introducing some current applications based on silicon nanomaterials such as light-based applications, photocatalysts and others in the energy field, we show the promising future of silicon in the nanofield.

2. Synthesis

Free-standing Si QDs can be synthesized by various routes including purely physical processes such as pulsed laser ablation, heating degradation and ball milling, chemical synthesis and the widely used electrochemical etching strategy. No matter which technique is used, research emphases are al-

*Project supported by the National Natural Science Foundation of China (Grant No. 212731126), the Fundamental Research Program of Shenzhen City, China (Grant Nos. JC201105201112A and JCYJ20120619151629728), and the Open Research Fund Program of the State Key Laboratory of Low-Dimensional Quantum Physics, China (Grant No. KF201311).

†Corresponding author. E-mail: sun.shuqing@sz.tsinghua.edu.cn

© 2014 Chinese Physical Society and IOP Publishing Ltd

ways placed on the particle dimensions, (narrow) size distribution, scalable production and well-controlled surface chemistry. In this section, we discuss several primary preparation and modification strategies to obtain the isolated Si QDs with sizes in the order of several nanometers.

2.1. Purely physical processes

2.1.1. Pulsed laser ablation (PLA)

Based on the precedents of using pulsed laser vaporization of the bulk metal within a pulsed supersonic nozzle to produce ultracold bare metal clusters of copper (Cu_2)[13] and even high-melting molybdenum (Mo_2),[14] nowadays the PLA method, which mostly uses a femtosecond or nanosecond laser pulse to irradiate the target Si wafer, has been substantially used to prepare semiconductor NPs especially Si NPs. By using argon–fluoride (ArF) excimer laser ablation under a constant helium (He) gas atmosphere (Fig. 1(a)), Yoshida *et al.*[15] indicated that the increasing size of Si NPs was in proportion to the rise in He pressure (Fig. 1(b)) on the assumption that the dissipated kinetic energy of the ejected material through the collision with the ambient gas atoms is related to the cohesive energy of as-formed crystallites. They applied this experimental phenomenon to an inertia fluid model. The relation between the diameter of ultrafine crystallite d_m and the ambient pressure p of the inert gas can be expressed as:

$$d_m \propto \sqrt[3]{\rho} \propto \sqrt[3]{p}, \tag{1}$$

where ρ is the density of the ambient gas .

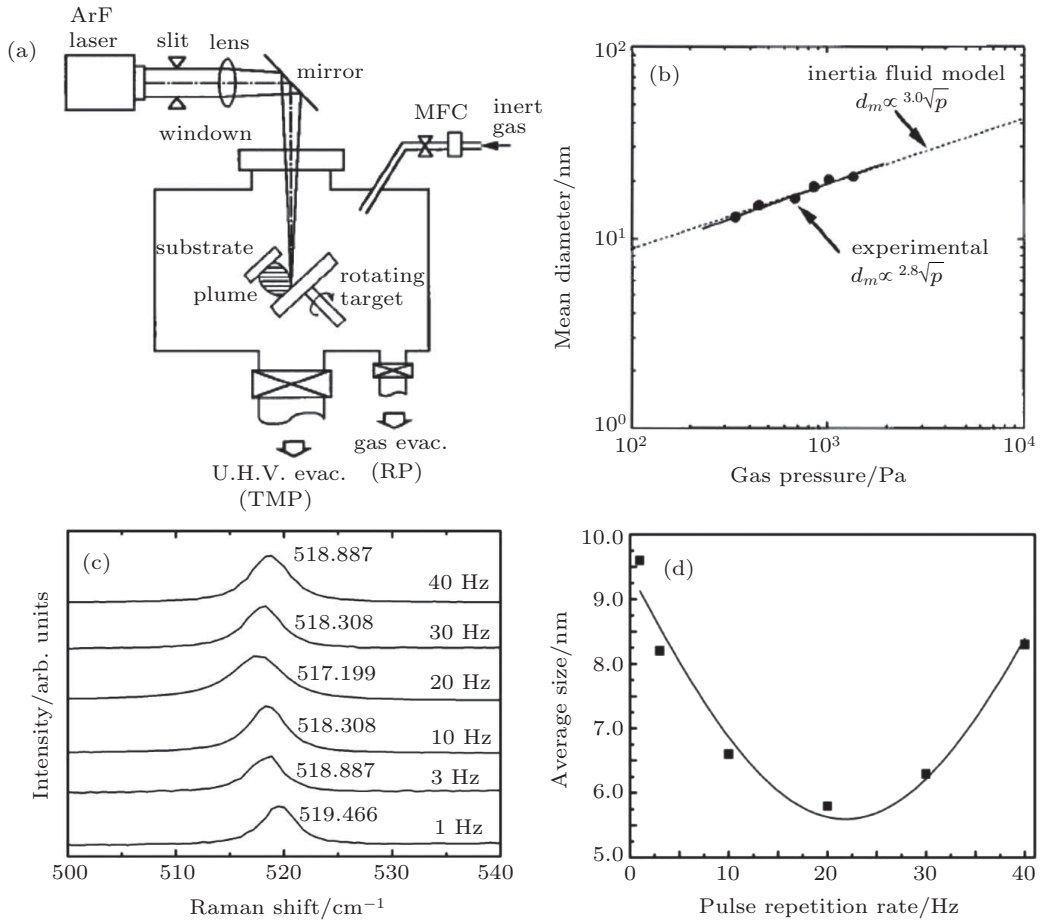


Fig. 1. (a) Schematic diagram of the preparation system of nanometer-sized Si ultrafine particles using ArF excimer laser ablation under constant pressure inert gas. (b) Mean diameter of Si crystallites as a function of helium (He) ambient pressure. The solid line represents the regression of experimental results. The broken line means the calculated results by the inertia fluid model.[15] (c) The Raman spectra of the samples prepared at 10 Pa of Ar at pulse repetition rates of 1, 3, 10, 20, 30 and 40 Hz. (d) The average size of nanoparticles in the films versus pulse repetition rate.[16]

Besides exploring the correlation between ambient gas pressure and particle size, other irradiation factors which may affect the process of nucleation, growth and aggregation of particles, such as repetition rate, pulse duration and energy are also taken into account. Wang *et al.*[16] performed Raman characterization (Fig. 1(c)) on samples prepared under different pulse repetition rates ranging from 1 Hz to 40 Hz and confirmed a nonlinear relationship between the repetition rate and the average size of Si NPs (Fig. 1(d)): when the pulse repetition rate is higher than the duration of the ambient restoration, the ablation dynamic process of the latter pulse is essentially affected by the remaining surroundings, thus various pulse in-

tervals might lead to different particle sizes. Kuzmin *et al.*[17] found that by using an argon (Ar) laser to ablate a target silicon immersed in ethanol, the mean particle size varied directly with pulse duration which may partially be related to the rapid effects of electronic relaxation inside the Si lattice and the viscous interaction of the molten layer with the expanding vapors of the surrounding liquid. Intantaglia *et al.*[18] successfully produced Si NPs with average sizes of 65 nm and 5 nm with the condition that the irradiation pulse energies used are 0.4 mJ and 0.15 mJ, respectively, to explore their distinctive optical properties. Moreover, other methods involving post-treatment have been tried to limit the dimensions of NPs. Abderrafi *et al.*[19] successfully synthesized small-sized Si NPs utilizing a two-step method which utilised nanosecond laser ablation of the Si wafer in chloroform ($CHCl_3$) followed by ultrasonic treatment in the presence of a mixed solvent which contained isopropanol, hydrofluoric acid (HF) and hexane (3:1:3). There is no doubt that HF plays an important role in reducing particle size, for it is responsible for preventing coagulation and removing the Si oxide surface.

By using a femtosecond laser system, Intartalia *et al.*[20] worked out a more convenient *in-situ* synthesis route to obtain DNA-bio-molecular conjugated Si NPs. Single-stranded oligonucleotides (SSO) were placed into deionized water followed by submerging the Si bulk in this biomolecule solution and then ablation was carried, with the parameters optimized in order to generate SSO-conjugated Si NPs efficiently. The average size of Si NPs can be reduced from 60 nm to 5 nm due to the 'growth quenching' caused by electric repulsions and steric hinderance between negatively charged SSO molecules on the surface of Si NPs.[21]

Many researchers prefer to use PLA to prepare Si nanocrystals because the particle size is easily tunable by controlling the experimental parameters and without requiring other chemicals. It is straightforward and clean since it is carried out on a bare Si wafer or immersed in water or polar solvents. However, low production efficiency cannot be overlooked.

2.1.2. Heating degradation

Many research groups have already focused on the thermal decomposition of silane precursers to obtain Si NPs and are keen to explain the internal nucleation mechanism. Two decades ago, Ho *et al.*[22] tried to synthesize Si atoms by using a rotating disk chemical vapor deposition reactor and simultaneously demonstrated that the primary Si atom production route can be demonstrated by two equations. After that, Swihart and Girshick[23] extended the Si atom number to 20 and systematically described a set of kinetic mechanisms for silicon hydride formation. Based on these fundamental researches, recently, researchers have proposed the formation of sterically stabilized silicon nanostructures featuring the freedom of environmental contamination under the conditions of heating and pressurizing in solvents under a higher temperature than their critical point ranging from 400 °C to 500 °C which could fully degrade organosilane precursors.[24] Otherwise microwave-assisted solutions have also been mentioned since silane is susceptible to thermal dissociation at certain microwave powers.[25] Knipping *et al.*[26] realized pure Si single crystals with particle sizes ranging from 6 nm to 11 nm by using microwave-induced decomposition of silane. According to their experimental results, the particle size was proportional to the precursor concentration, but total gas pressure was inversely proportional to microwave power. To date, this method has been used to synthesize many nanostructures.[27,28] For example, Si NPs featuring blue emission, great PL yield, high pH stability and favorable size were prepared by a facile one-pot aqueous synthesis. In this process, microwave heating is an important factor for both nucleation or Oswald ripening.[29] Compared with typical heating processes, the microwave-assisted method has more advantages such as the uniform heating of solvents, the greater selective heating of reactants, and specifically, a shorter reaction time that can be shrunk to the order of minutes instead of a couple of hours, owing to the efficient absorption of microwaves, thereby greatly accelerating the reaction rate.[30]

2.1.3. Ball milling

In this way, Lam *et al.*[31] produced Si NPs with dimensions of about 5 nm by pure mechanical attrition of solid graphite (C) with silicon dioxide (SiO_2) in a planetary ball miller for 7–10 days followed by annealing at 150 °C. The resulting NPs were capped with an amorphous Si oxide layer about 1 nm in thickness and featured a multi-peak PL spectrum, owing to the broad range of particle sizes. Besides the wide size distribution, aggregation was also a serious problem because this led to a complex and coarse shape. Due to these drawbacks, nowadays it is rarely used compared with other physical synthetic strategies though it is convenient and inexpensive.

2.2. Physicochemical methods

The most typical physicochemical method is photothermal aerosol synthesis, especially laser-induced decomposition of gas phase precursors. Generally, laser-induced dissociation of Si precursors is composed of three steps. Firstly, the silicon powders were synthesized by CO_2 laser-induced heating of silane accompanied by hydrogen and a photosensitizer (e.g. sulfur hexafluoride) to a degree that it can be effectively dissociated. The size of the resulting silicon powders ranges from 5 nm to 10 nm[32] or even larger than 10 nm,[33] that cannot manifest a strong size confinement effect, that is, they have a much lower PL efficiency. Because of this, a post treatment to obtain size selection and to reduce particle dimensions is necessary. Based on the theory that the velocity of the nanoclusters correlates with their mass, in other words, cluster

size, a slotted molecular-beam chopper wheel can help to select neutral clusters as discussed by Ehbrecht and Huisken.[33] In another aspect, many groups focused on the etching of the obtained Si NPs using HF/HNO_3 to induce bright visible luminescence.[32,34,35]

Unlike a physical route which leads to a low-product yield, in this way, gram scale quantities of Si QDs can be produced[36] featuring non-aggregation, well-controlled nanoparticle size, and deposited on to any desired substrate or liquid medium. For example, Huisken *et al.*[37] performed particle injection through a nozzle into a high vaccum device and then deposited a molecular beam of Si clusters on a suitable substrate.

2.3. Chemical techniques

Initially, solution phase synthesis of Si NPs was accomplished by Heath.[38] Silicon halides are employed as a starting material. The reduction of silicon halides by various reducing agents (e.g. sodium naphthalenide,[10,38,39] lithium naphthalenide,[40] lithium–aluminum hydride[41,42] or zintl salts[43]) in a variety of surfactant solvents can result in small-sized, free-standing Si NPs, and the resulting Si NPs are generally hydrogen-capped.[41,44] Recently, by using allyltrichlorosilane as both the surfactant and the functionalization reagent and silicon tetrachloride in a ratio of 1:3, our group explored a simple approach to the synthesis of morphology-controlled hexagonal silicon nanocrystals modified with allyl in the range of 20–50 nm (Figs. 2(a) and 2(b)). The Si–Cl bonds were reduced by lithium tetrahydridoaluminate to Si–Si which promotes the growth of Si crystals.[45] To control the size dispersion, Tilley and Yamamoto found that the narrow size distribution could be obtained by using powerful hydride reducing agents and selective surfactants in micelles, which is termed 'micro-emulsion synthesis'.[46] In this process, the surfactant plays a critical role in restricting the core growth and finally resulted in uniform particle dimensions. In our group, we demonstrated a one-step technique to produce highly monodispersed, alkyl-capped, brightly luminescent nanocrystals (Fig. 3(a)) using hexyltrichlorosilane as both the surfactant and the reactant. Compared with the experiment without hexyltrichlorosilane, this reaction system resulted in smaller Si QDs with diameters of 2 ± 0.5 nm, which showed a relatively narrow size distribution and excitation wavelength-dependent PL performance as shown in Fig. 3(b). The PL peaks range from 350 nm to 450 nm as the excitation wavelength is red-shifted.[47] Besides this method, other reaction precursors have also been used in similar processes. When zintl salt with ammonium bromide was used, nanoparticles with bright blue emission in the size range of 3.9 ± 1.3 nm could be obtained accompanied by several byproducts such as ammonia, hydrogen, and sodium bromide.[48–50]

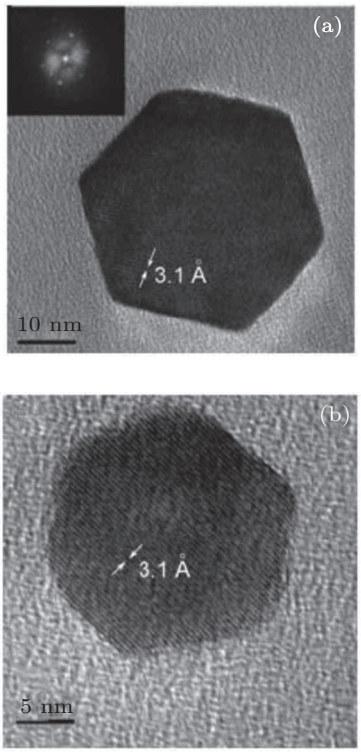


Fig. 2. (a) HRTEM image of a 50-nm silicon crystal, inset: Fourier transformation result. (b) HRTEM of a 20-nm silicon crystal.[45]

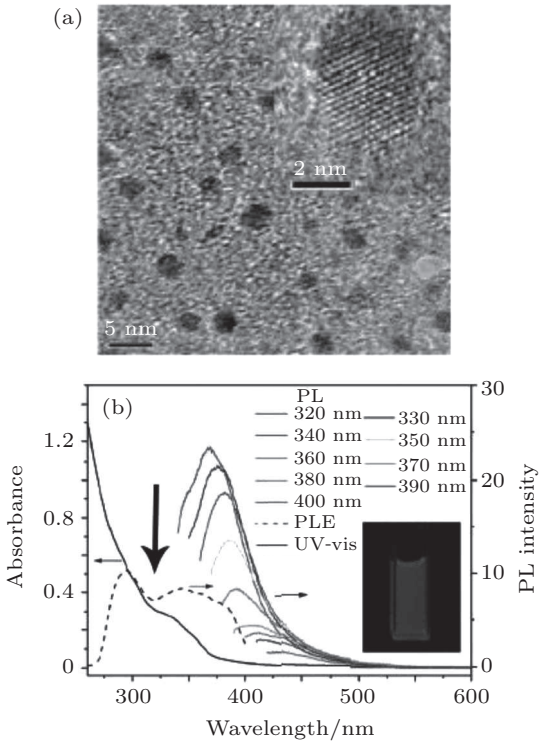


Fig. 3. (a) TEM images of hexyl-capped Si QDs obtained from the reduction of hexyltrichlorosilane/$SiCl_4$ micelles, inset of panel (a): an HRTEM image of an individual silicon nanocrystal. (b) Room temperature UV–vis absorbance, excitation wavelength dependence of PL emission, detected at 420 nm of PLE spectra of hexyl-capped silicon nanocrystals dispersed in hexane. As indicated by the arrow in the picture, the intensity of the PL spectrum becomes weak as the excitation wavelength is red-shifted from 320 nm to 400 nm. Inset: the photograph of the obtained Si QDs dispersed in hexane under illumination of UV light.[47]

2.4. Electrochemical techniques

Although there are a number of methods to obtain silicon nanoparticles, perhaps an electrochemical technique can be regarded as the most convenient route. Empirically, galvanostatic anodization was utilized to form porous silicon (PSi) termed 'silicon nanocrystal thin film' which was the origin of photoluminescent Si NPs. The traditional procedures of this method are to fill a Teflon cell with a mixed solution of aqueous HF and ethanol followed by etching a silicon wafer with a constant current source, then to carry out a fracturing treatment (e.g. sonication) on the freshly etched PSi layer to obtain the quantum confined colloidal silicon nanoparticles.[51–55] According to this well-established procedure, many factors (e.g. electrolyte composition, etching time, silicon dopant type and dopant concentration)[56] may irreversibly affect the surface morphology and properties of the PSi thin film. The role of ethanol is to prevent the bubble from splitting and to overcome the strong hydrophobic nature to make the pores continue propagating,[57] thus more uniform hydrogen-terminated silicon nanocrystals can be generated.

2.5. Strengths and weaknesses

As has been discussed before, size control of Si NPs prepared by physical methods is simple without using chemical reagents, however, it cannot realize scalable production and the obtained Si QDs need further modification to stabilize. Unlike physical methods, by chemical recipes, synthesis, surface modification as well as controllable particle size distribution of Si QDs can be achieved simultaneously under mild conditions.[10,41] However, contamination of residual byproducts such as the reducing agents is compromised. In another part, porous silicon, produced by the electrochemical procedure under certain conditions, can be used as a source of Si QDs and is always regarded as primary material for Si QDs due to both the high yield[51] and uniformity in essential properties.[58] However, the lack of capability to control particle size, shape and size distribution is a noticeable drawback of this method, which needs a further separation process.

2.6. Surface modification

The chemical reactivity of the nanoparticle surface is much higher than that of its bulk counterpart. In most cases, pristine Si nanocrystals with hydrogen-termination are metastable and the surface is hydrophobic, sensitive to oxygen and water. Surface modification of Si nanocrystals with a variety of functional molecules can significantly improve their stability and optical performance,[59,60] and at the same time can afford solubility in a wide range of solvents.

According to Refs. [61]–[63], the existence of dangling bonds on the surface of Si NPs enhances the reactivity with other organic molecules, for it contains one instead of two spin-paired electrons. There manifests a tendency toward minimizing the free energy, in other words, to eliminate the dangling bonds. The energy minimization is a trade-off between the energy gained by forming new local bonds and the energy lost because of bond strain that results from its new configuration, and it leads to complex reconstruction of the surface which may evolve into termination with certain molecules.

To date, different types of water-soluble Si NPs with bioconjugation are available for various applications both *in vivo* and *in vitro*. The derivation occurs not only on an Si–H bond which can be easily oxidized, but also in a weaker Si–Si linkage. Several techniques have been employed to accelerate this process under an inert atmosphere which is inevitably needed whenever most procedures are manipulated in order to prevent the surface from being oxidized.[64] The chemically stable Si–C bond has been regarded as an ideal candidate for a perfect medium for further chemical compound (e.g. acrylic acid, octylamine,[48] 4-bromo-1-butene,[64] epoxide,[65] 1-heptene[66]) passivation due to its low polarity and high bond strength through hydrosilylation, or for further modification, in which the small organic molecules with a C=C end group are used to form hydrophobic and hydrophilic Si NPs.[46,51] There have been some investigations on *in-situ* oxidation under high temperature to form a SiO_2 layer that enables the particle to become water-soluble and easy completion of surface functionalization attributed to the polarization effect.[67] Here, we review the most commonly used approaches to the hydrosilylation of silicon nanocrystals, including metallic catalysis, UV irradiation, heating treatment and microwave-assisted functionalization.

2.6.1. Metallic catalysis

So far, the platinum catalysis method has been regarded as a superior approach to modifying the Si nanocrystals, for it can be completed under ambient temperature. Generally, the reactive hydrogen-terminated silicon nanocrystals are treated with an amphiphilic polymer with C=C double bonds through platinum catalysis to form a stable Si–C bond followed by further surface fabrication.[11,41,42,46,48,51,65,68] Compared with treating the surface with Grignard reagents or forming Si–O groups, this method owns the capability to cap the surface with alkyl chains containing functional groups without restriction on available reagents and to overcome the effect of electric charge distribution due to the existence of the Si–O bond.[46,69]

2.6.2. UV irradiation

In this case, UV illumination for a couple of hours is necessary, which is responsible for the adverse effects on the specific optical properties of Si NPs, however, it can ef-

fectively avoid the inducement of impurities. For example, Li and Ruckenstein[70] have successfully synthesized water-dispersible Si NPs terminated with acrylic acid, showing strong PL stability under UV irradiation. Sato *et al.*[60] also changed the termination of the surface of Si NPs from hydrogen to propionic acid (PA) by mixing the Si nanocrystals and the solvent of acrylic acid and hydrofluoric acid under photoinitiation. Thus they obtained water-dispersible Si NPs that show strong luminescence of various colors.

2.6.3. Heating inducement

To meet the requirement for bio-application and improve the stability of Si NPs, silicon/silica core/shell nanostructure or covalently attaching hydrophilic molecules to the surface is necessary. Secret *et al.*[71] prepared anionic porphyrin-grafted porous silicon nanoparticles with sizes ranging from 35 nm to 245 nm in two steps: hydrosilylation with allylisocyanate at 90 °C for 2 h followed by grafting with porph-NH_2 through an amine group at 80 °C for 18 h, allowing the delivery of porphyrin drugs into cancer cells. Besides the native oxidation, researchers are inclined to carry out controllable oxidation. A case using this method is the thermal oxidation of porous silicon which consists of numerous silicon single nanocrystallines. As done by Gelloz and Koshida,[72] the samples were treated under the condition of 900 °C for 30 min followed by high-pressure water vapor annealing, thus resulting in silicon nanocrystallite with a passivated SiO_2 shell, featuring blue-band phosphorescence with a long lifetime.

2.6.4. Microwave-assisted functionalization

Recently, by using a microwave-assisted method in both the procedures of synthesis and surface modification, Shafeev *et al.*[25] reported that they have successfully produced 3-aminopropenyl-terminated Si NPs featuring strong PL peaks in the visible blue region accompanied by a high quantum yield of 15%. Using this method, our group produced decene, undecylenyl alcohol and undecenoic acid functionalized Si QDs (Fig. 4(a)). The results manifested a similar broad absorption band to the original hydrogen-terminated one. Correspondingly, the fluorescence emission peaks of hydroxyl-terminated and carboxylic acid-terminated Si NPs in water were centered at 670 nm and 680 nm, while decene modified Si QDs exhibited a blueshift due to Si–O defects (Fig. 4(b)). The rate of hydrosilylation is remarkably fast, for the procedures could be accomplished in only 15 minutes and can achieve high surface coverage simultaneously.[52] Because of the high temperature surroundings, it is crucial to control the reaction conditions in order to prevent the modification substance from deteriorating, such as with protein degradation.[73]

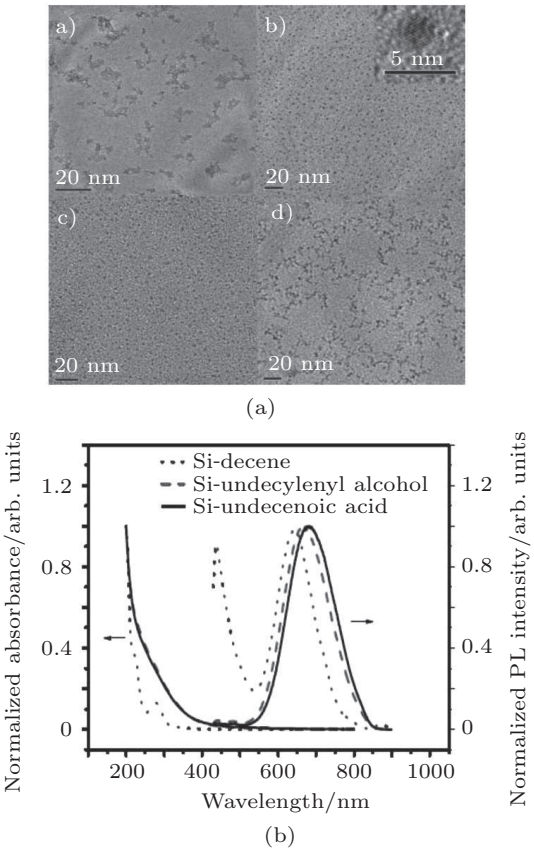


Fig. 4. (a) TEM images of a) freshly prepared hydrogen-terminated silicon nanoparticles, b) undecylenyl alcohol functionalized Si QDs (inset: high-resolution TEM image of an individual silicon nanocrystal), c) undecenoic acid functionalized Si QDs and d) decene functionalized Si QDs. (b) Absorption and PL spectra of decene, undecylenyl alcohol and undecenoic acid functionalized Si QDs. PL is measured using ultraviolet excitation ($\lambda = 365$ nm).[52]

2.6.5. Strengths and weaknesses

The modification of the surface has certainly contributed to the utilization of quantum-confined Si nanocrystals in many special fields. All modification methods have their own limitations. Since the process is simple and can be completed under ambient temperature, the metal catalysis reaction has been widely used, however, the catalyst may stubbornly attach to the surface of the resultant NPs. To improve this, UV irradiation is preferred as it can get rid of platinum NP contamination[74] and only a short time will be needed when compared with heating inducement and metal catalyst process, and may extensively reduce the risk of inducing the decrease of fluorescence efficiency. Microwave-assisted hydrosilylation also owns noticeable merits including simpler workup procedures, higher surface coverage and stability, milder conditions without using any toxic precursors, an in particular, a shorter reaction time in the order of several minutes.[25,29,30]

3. Properties

3.1. Optical performance

Due to the low PL quantum yield (QY) of amorphous Si NPs, which is less than 2%,[64] most researches focused

on the size-dependent and efficient PL of Si nanocrystals. The special optical properties, including bright emission, photo-stability, size-dependent and wavelength-tunable luminescence, and long fluorescence lifetime make them suitable for many applications.[32,67] Although so far, the origin of PL is controversial and this question has no satisfactory answer, there is a consensus that the PL is generally determined by two aspects: one is due to the quantum confinement effect which may be the consequence of size quantization of the Si nanoparticle skeleton structure,[75] and the other is assigned to localized states surrounding the nanoparticles.[76,77] In the quantum confinement region, the PL property is closely dependent on dot size which is more important than surface chemistry in predicting the electronic properties of surface-passivated nanostructrues,[78] even with a 0.1-nm change, which may lead to apparent differences in emission band energy.[67] The PL peak will be red-shifted with size, increasing up to a size point larger than the critical size point. Ledoux *et al.*[79] explained the relationship between optical peak energy and particle size based on the quantum-confinement model using a linear combination of atomic orbitals (LCAO) (Fig. 5(a)), which has a recombination energy of the electron–hole pair (E_g), has a blue-shift with respect to the band gap of bulk Si ($E_0 = 1.17$ eV) and obeys an inverse power law with an exponent of 1.39 for the diameter (d) measured in nanometers (solid line in Fig. 5(a))[75]

$$E_g(\mathrm{eV})(d) = E_0(\mathrm{eV}) + \frac{3.73}{d(\mathrm{nm})^{1.39}}. \quad (2)$$

Most part of the experimental data are in good accordance with the theoretical ones except some distinctions between data and theoretical results at both ends. For small particles, the deviation is attributed to the finite size distribution and the existence of an oxide-related surface state within the band gap of the Si nanocrystals.

Meanwhile, size dispersion is also a crucial factor, owing to the fact that when the size distribution becomes wider, the PL intensity will turn lower.[80] Meier *et al.*[81] systematically explored the influence of size distribution on optical emission performance. By using the equation:

$$I(\hbar\omega) = \int_0^\infty f_{\mathrm{osc}}(\tilde{d}) \frac{d_n(\tilde{d}, d_0, \sigma)}{d\tilde{d}} I_{\mathrm{NP}}(\hbar\omega, E_{g,\Delta E}(\tilde{d}))\,\mathrm{d}\tilde{d}, \quad (3)$$

where σ is the geometric mean deviation of Si NPs, f the oscillator strength, $\hbar\omega$ the photon energy, ΔE the spectral width of a single NP at room temperature, which acts as an inhomogeneously broadened emitter, and I_{NP} the PL intensity for a single particle, Meier *et al.*[81] computed the PL emission of a NP ensemble with an average particle diameter d_0, and they found that the model calculation fitted well with experimental data. So based on this, they kept the particle size d at a constant value and found the influences of ΔE and σ on PL performance, which are shown by Fig. 5(b): the PL spectral shape is very sensitive to the particle dispersion σ, even only a difference of 0.05 may lead to a significant change in PL performance, that is, for small NPs, size distribution is an indispensable factor in deciding the PL.

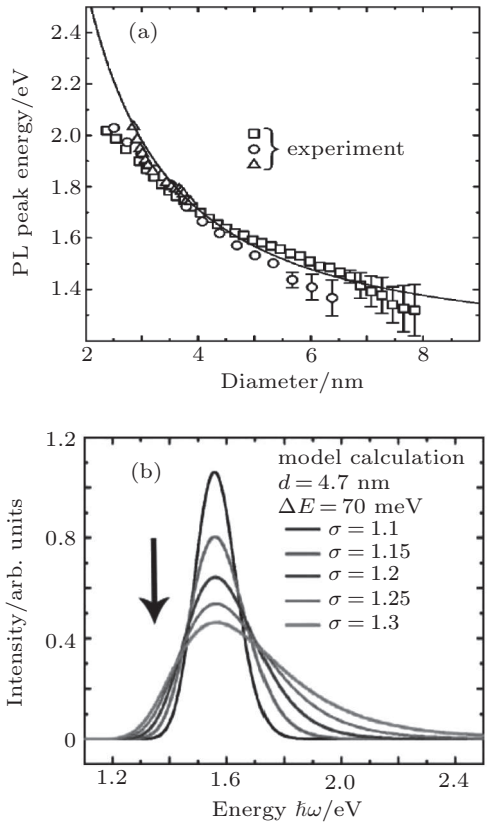


Fig. 5. (a) Correlation between average diameter and PL peak energy. The solid curve represents the theoretical data, squared data and the two other data set points are obtained from the sample resulting from similar experiments.[79] (b) Correlation between the geometrical standard deviation on the ensemble PL spectral.[81] As indicated by the arrow, the width and intensity of the spectrum becomes wider and weaker, respectively with the dispersion of particle size increasing in the range 1.1 to 1.3.

It has been widely known that the presence of oxygen or some other elements such as nitrogen can induce dramatic changes of PL properties.[82,83] Recently, by capping $\sim$ 3-nm hydrogen-terminated Si QDs with an oxide layer in (EtOH)/H_2O_2 solution, Kang *et al.*[67] were able to synthesize the Si cores in different sizes with a SiO_xH_y shell and showed a marked blueshift of emission wavelength from salmon pink to blue (Figs. 6(a) and 6(b)). Oxidizing the hydrogen-passivated surface of Si QDs in different times ranging from 0.5 h to 24 h led to diameter divergence from 3.0 nm to 1.2 nm (Fig. 6(c)), Kang *et al.*[67] concluded that with increasing oxidation time, the Si core size significantly decreased which was responsible for the finely wavelength-tunable emission photoluminescence. After the oxidation treatment, the PL QYs increase since the nonradiative surface states are removed by the native oxide and simultaneously the emission energy shifts toward a higher band, accompanied by the shrinkage of the silicon crystalline core as a result of the surface oxidation.[84–86] Through

slowly heating or photoinitiating, a SiO_2 layer formed which was responsible for the conversion of emission colors.[87] By post-treatment of high-pressure water vapor annealing after oxidation passivation, the intensity of blue emission can be efficiently enhanced due to the inducement of the high quality of the Si–O–Si bridge or Si/SiO_x interfaces.[72] Besides, trace nitrogen may also contribute to blue emission. Dasog *et al*.[88] found two situations in which no blue PL was observed from the presented Si NPs synthesized by hydrofluoric acid etching of Si/SiO_2 and they attributed this phenomenon to a charge-transfer-based mechanism raised by Nekrashevich and Gritsenko[89] who explored the electronic structure of silicon oxynitride. In view of their various fabrication methods, Si nanocrystals can lead to different origins of blue PL. Yang *et al*.[90] demonstrated that Si NPs prepared by laser ablation in a liquid could emit blue light and featured aging-enhancement. They included a set of processes to explain the mechanism of blue light emission instead of a mere quantum confinement effect, that is, excitons were first formed through direct transitions at the Γ or X point by the absorption at 365 nm or 270 nm, and then partly trapped in nonradiative Pb centers, the others migrated to the near-interface traps at the interface between Si and SiO_x ($0 < x < 2$). Besides the effect of particle size, size distribution, and an added element such as oxygen and nitrogen, surface characteristics can also lead to distinct changes of the optical properties of Si NPs. By capping the surface with various functional groups,[29,91] compared with organic fluorophores and polysilanes, Si NPs maintain stable PL for a longer lifetime which means it can effectively resist against photobleaching. By comparing hexyl, octyl, dodecyl and octadecyl capped Si NPs, researchers found out that there was no obvious difference in optical properties among them when using different length chains.[92] Moreover, there were also some cases concerning PL enhancement through surface modification. Through surface derivation of diphenylamine and carbozale separately, Li *et al*.[93] produced ultra-bright Si QDs with the stable QYs up to 50% and 75%, respectively, due to a single highly emissive recombination channel across the entire NP ensemble induced by the modification. Meanwhile, the emission peak was red-shifted from 405 nm to 500 nm. In contrast, (3-aminopropyl) triethoxysilane (APTES) derived hydroxyl-terminated Si NPs presented a distinctively attenuating PL intensity and a blueshift due to the polarity characteristic of amino group. The QYs of Si NPs conjugated with different functional groups are summarized in Table 1.

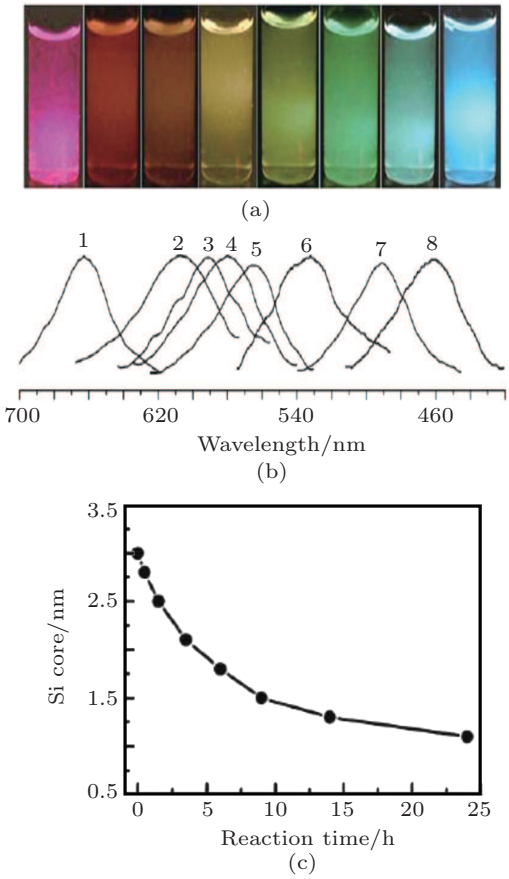


Fig. 6. (color online) (a) Photograph (under UV light) of H–Si QDs (left, red emission) and seven water soluble Si QDs (yielding seven distinct emission colors). (b) PL spectra of H–Si QDs (curve 1) and Si QDs after 0.5, 1.5, 3.5, 6, 9, 14, and 24 h oxidization (curves 2–8), respectively (excitation wavelength: 360 nm). (c) Plot of the oxidation time versus Si core size.[67]

Table 1. QYs of Si NPs conjugated with different functional groups.

Functional group	Synthesis route	PL QY/%	Size distribution/nm	Medium solution
Octasiloxane[10]	reduction of $SiCl_4$	12	3.28±0.86	hexane or chloroform
Allylamine[41]	reduction of $SiCl_4$	10	1.5±0.5	water
Octylamin[48]	reduction of zintl salt	18	3.9±1.3	water
3-aminopropenyl[30]	microwave-assisted reaction in liquid	15	3.4±0.7	water
Immunoglobulin G (a protein)[73]	microwave-assisted reaction in liquid	18	3.17±0.53	water
Dodecyl[87]	reduction of micelle	14	6.05±1.94	hexane
Aminoalkyl[51]	microwave-assisted reaction in liquid	20–25	2.2±0.7	water
Octanethiol[24]	degradation of organosilane	5.5	4.64±1.36	water

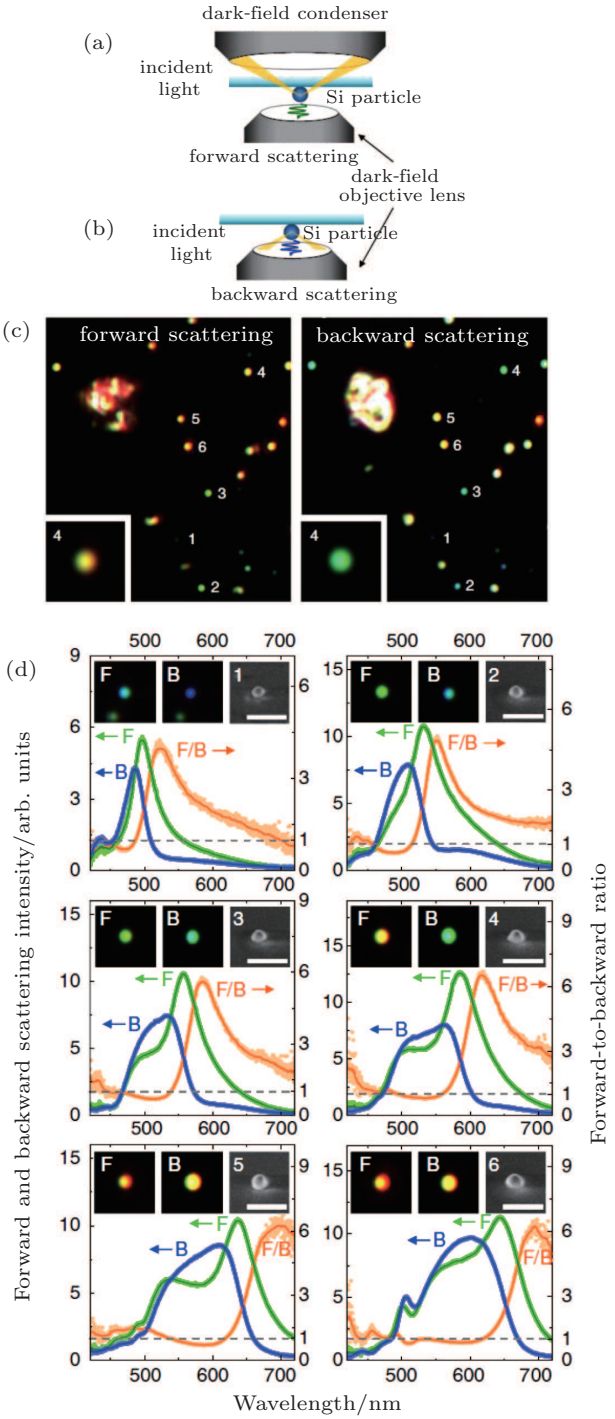


Fig. 7. (color online) (a) and (b) Schemes of forward and backward scattering measurements. (c) True colour CCD (charge-coupled device) images of the forward and backward scattering by Si nanoparticles. Inset in panel (c) shows magnified dark-field microscope image of nanoparticle #4 in forward and backward scattering directions. (d) Left axes show forward (green) and backward (blue) scattering intensities, and right axes show forward (F)-to-backward (B) ratio (orange curves) of silicon nanoparticles selected in panel (a). Dashed lines represent the forward-to-backward ratio equal to unity. Dots represent experimental data, and solid lines are computer-smoothed. Insets show close view transmitted (F) and reflected (B) dark-field microscope images, and SEM images taken at an angle of 52 for each selected nanoparticle (1–6). The scale bar in the SEM images is 500 nm.[97]

Nowadays, nanocomposites (e.g. Si NPs/magnetite, Si NPs/silver) have attracted considerable attention, for their multi-functionality is superior to either component. Mertens *et al.*[94] have synthesized Si NPs coupled with silver rods, and the nanostructure can extremely enhance the PL intensity which is attributed to the electromagnetic coupling of the Si QD emission dipoles with dipolar plasma modes in the silver rod. Iron-doped porpylamine-terminated Si nanoparticles have been fabricated for both photoluminescence and magnetic resonance imaging (MRI) detection. In this study, a sample containing the least quantity of iron (Si_{1Fe}) exhibited the highest QYs (15%); a higher concentration of iron dopant (Si_{5Fe}) caused fluorescence attenuation (10%),[95,96] whereas MRI T_2 contrast increased. Besides the influence of iron content, it has been found that the size of the hybrid is another significant factor influencing the intensity of PL.[96]

Besides the controllable PL, recently, directional anisotropic scattering in the visible spectral range of Si NPs has been explored in depth, in order to apply Si NPs to some emerging nano-scaled applications. Based on the theoretical modeling by using Mie theory, Fu *et al.*[97] synthesized approximately spherical Si NPs solidified on glass substrates with thickness values ranging from 100–200 nm and systematically analyzed the scattering performances in the forward and backward directions (Figs. 7(a) and 7(b)). As shown in Fig. 7(c), labeled samples manifest various scattered colors in two directions due to simultaneously excited electric and magnetic dipoles. By comparison with the measured spectral behavior of the six Si NPs (Fig. 7(d)), Fu *et al.* also confirmed that the quasi-spherical Si nanocrystals could act as 'Huygens' sources and the spectral region was tunable since the scattering resonances was merely linearly dependent on the particle size and wavelength of the illumination light.

3.2. Electronic properties

Generally, special PL properties of Si NPs are primarily due to the quantum confinement effect caused by the restricted size at the nanoscale. The existing quantum confinement model is closely related to the size-dependent band gap which is also one of the major characteristics of electronic nature. According to the research results presented by Van Buuren *et al.*,[98] after synthesizing Si NPs with a fair size range from 1–5 nm, they found that the valence band (VB) edges of the Si nanocrystals shifted down by 0.5 eV with respect to vacuum level, owing to electronic structure changes caused by quantum confinement. Moreover, the conduction band (CB) shift was measured as a function of the VB band shift which is quantitatively equal to twice the former. They confirmed the inverse relation between particle size instead of geometric shape and the size of the band shift. However, the calculated band gap did not perfectly match the measured one due to the partially oxidized surface and substrate–cluster interaction. In addition to the marked effect of particle dimension

on electric performance,[78,98–100] the type of dopant (phosphorus or boron),[101] composition material,[102–104] surface functionalization[105] and post treatment[106] similarly manifest noticeable effects. For example, by comparing the electronic transport of Si NCs networks using films composed of P-doped Si–NCs with those using films consisting of Si NPs without doping elements, Stegner *et al.*[101] found that the dopant can strongly influence the electronic transport properties of the films. For the undoped film, thermal activation energy (E_a) was about 0.5 eV and the increased dopant concentration led to the relationship that conductivity increases and conductivity decreases as temperature rises. Apart from these, Kim *et al.*[107] adopted plasma-enhanced chemical vapor deposition (PECVD) followed by annealing to insert Si NCs into amorphous silicon nitride to prepare silicon-based solar cells. However, the large spacing between Si NCs in silicon nitride film brought about lower light absorption-induced photocurrent than the theoretical value, from which one can conclude that the spacing relationship between Si nanocrystals was also a remarkable factor influencing the electric properties.[107]

4. Applications

4.1. Light-emitting applications

For light-emitting applications using Si NPs, most of them rely on their robust electroluminescence (EL) potential. The realization of this application demonstrated that through optimizing the confinement of holes and electrons of the nanocrystal layer, the semiconductor material can also be used in this field.[108,109] Work by Maier-Flaig *et al.*[110] showed that through using monodispersed size-separated silicon nanoparticles, multicolor silicon-based light-emission diodes (Si LEDs), featuring long-term stable EL as well as widely tunable colors ranging from deep red to orange–yellow, can be achieved. The Si NPs proved to play a pivotal role since the emission characteristic substantially originates from it through the comparison between EL and PL spectra. Moreover, the increasing external quantum efficiency (EQE) is partially determined by the reduced thickness of the Si NP layer and the high wavelength emission of Si nanocrystals. Meanwhile, comparative trials have been carried out between samples with and without size selection. The results showed that a longer operation time of the device results in superior particles as indicated by the comparison between 40-h and 15-h operations. Simultaneously, the products with selected Si NPs could realize small voltage-dependent wavelength shifts of the order of 15 nm when the applied voltage was increased from 3.5 V to 10 V, which is attributed to the residual size distribution. In addition, the device also displayed some particular merits, e.g. extreme brightness with the QYs up to 43%, low turn-on voltage of approximately 2 V for red-emitters, and thus paved a perfect way to new silicon-based optoelectronic applications.

4.2. Applications in the energy and electronic fields

Si NPs exhibit fascinating electronic and optical properties compared with bulk silicon and have been investigated in depth for photovoltaic applications.[111–113] For lithium-ion battery applications, silicon formulations such as silicon nanowires, silicon nanotubes and microporous silicon nanoparticles have been widely investigated[114–117] to overcome the disappointing shortcomings of previous silicon anodes. Despite the change in nanostructure, researchers have ceaselessly been searching for novel candidate anode materials featuring higher Li-ion storage and stronger rechargeable capability to serve as substitutes for low charge-stored carbon-based anodes. Recently, Guo *et al.*[118] focused on synthesizing a Si/C nanocomposite by infiltrating the Si NPs uniformly into the carbon matrix in order to excite its potential as anode material. To prove the superiority of this micron-sized mesoporous Si–C nanohybrid, delithiation capacity, coulombic efficiency (CE) and a charge/discharge process were systematically discussed. The resulting curves show that, except for the depressing irreversible capacity for the initiate cycles with a CE of only 22.3%, with the increase of cycle number the delithiation capacity shows a desirable increasing tendency until the 70th cycle, after which it maintains a high level constantly. Researchers attributed this phenomenon to the partial existence of a SiO_x layer, through which the Si NPs can disperse in the carbon precursor homogeneously. Despite the manifestation of deformity in the first cycle, this lithium battery anode in which Si NPs plays a vital role is a significant leap in this field for its prominent cycling stability and high reversible capacity.[118] Ge *et al.*[119] synthesized a novel graphene oxide-wrapped carbon coated porous silicon nanoparticle anode featuring better cycle-ability and less capacity degradation, for it could operate at much higher current rates of 1/4 C and 1/2 C and deliver extremely stable capacities of 1400 mA·h/g and 1000 mA·h/g after 200 cycles, respectively (Fig. 8).

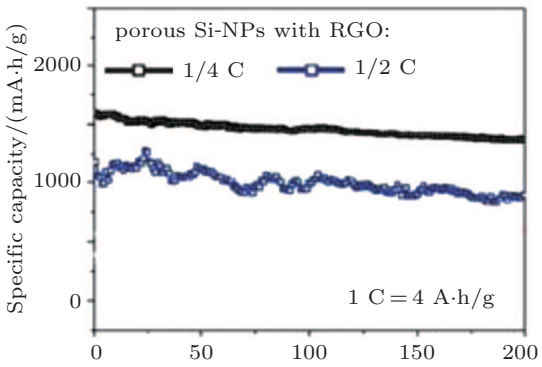


Fig. 8. (color online) Cycling performances at current rates of 1/4 C and 1/2 C.[119]

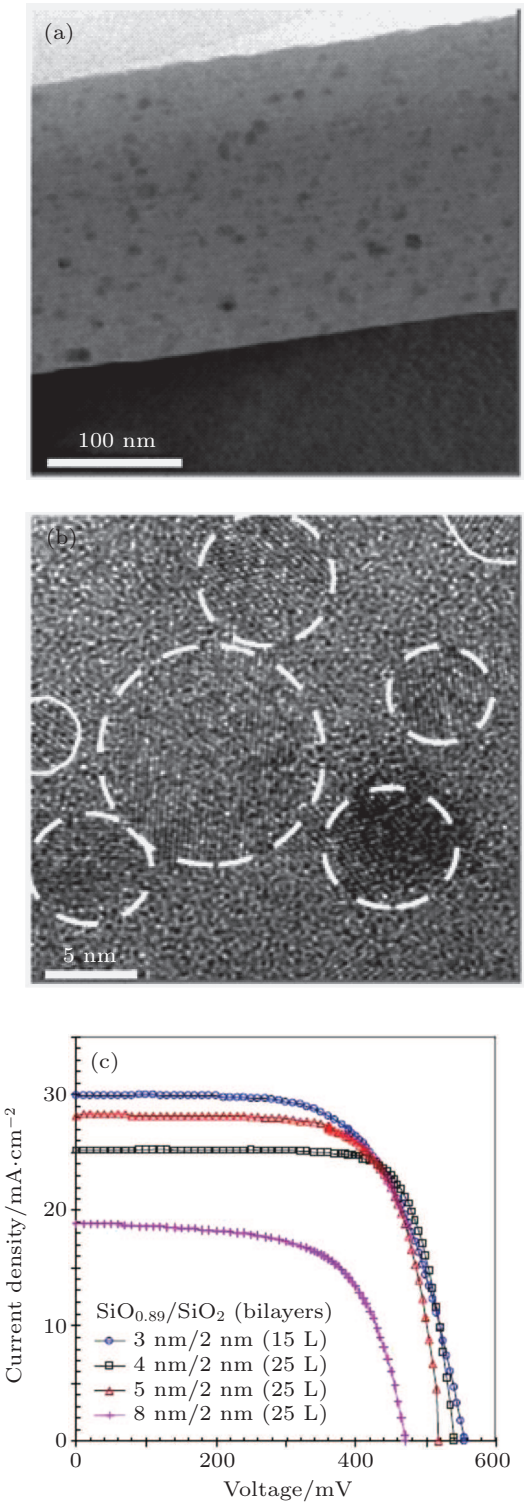


Fig. 9. (color online) TEM images of Si QDs in an SiO_2 matrix, (a) low-magnification image and (b) high-resolution image. (c) One-sun illuminated *I*–*V* curves of four different (n-type) Si QD/ (p-type) c-Si solar cells measured at 298 K.[113]

For solar cell battery applications, there are several nanostructured cell protocols to achieve higher conversion efficiency than those protocols based on a single p–n junction such as silicon-based tandem cells, hot carrier cells and up- and down-conversion.[111–113,120] Recently, Cho *et al.*[113] reported that they have successfully fabricated a phosphorus-doped Si QD superlattice as an active layer on a crystalline silicon oxide substrate as a heteroface solar cell. For its high solid solubility in silicon under high annealing temperature ($\sim$ 1100 °C), phosphorus was chosen to be the alloying element to form P-doped Si QDs by magnetron sputtering of Si, SiO_2 and P_2O_5 targets. The structures are shown in Figs. 9(a) and 9(b). Through comparing heteroface diodes with different Si NPs diameters, the cell with 3-nm QDs capped with a 2-nm SiO_2 layer was described as being superior for its higher open-circuit voltage (V_{oc}), short-circuit current (J_{sc}) and conversion efficiency under solar illumination over other counterparts (Fig. 9(c)).[113]

For electronic devices, since 1999 when Ridley *et al.* reported the first nanocrystal field-effect transistor (FET) prepared by using sintered CdSe NCs,[121] FET containing Si NPs have attracted great attention. Recently, there was a report concerning Si NPs thin-film field-effect transistors prepared from solution. In this article, Si NCs were synthesized in a nonthermal plasma via the dissociation of hydrogen and SiH_4; the resulting powder was dissolved in 1, 2-dichlorobenzene (DCB) followed by sonication, thus forming a stable suspension, though it was not optically transparent. To have a comprehensively understanding, germanium NP-based FET was also studied. The two kinds of bottom-gate FETs were fabricated by spinning them onto Au/Si^{2+}/SiO_2 substrates, the structure is shown in Fig. 10(a). Unlike the Ge-based apparatus, films of Si NCs of either 4 nm or 7 nm in diameter exhibit n-type behaviors (Figs. 10(c) and 10(d)), but have a nonuniform, discontinuous and visible rough surface (Fig. 10(b)), though it manifested poor performance, for the on-to-off ratio is approximately two orders of magnitude and the transfer curve shows significant hysteresis. It was the first time to realize deposition of Si NC thin films from solution which showed gating without any postdeposition treatment.[122]

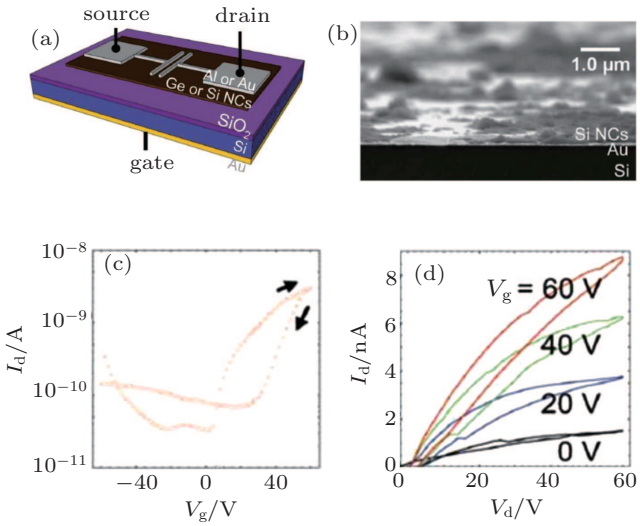


Fig. 10. (color online) (a) Schematic plot of FET device. The channel dimensions are 200 μm × 2000 μm and the source is grounded during operation. (b) A 7-nm-thick Si NC film on an Au-coated Si wafer. (c) Drain current (I_d)–gate voltage (V_g) for two different 10–20 nm as-deposited Si NC FETs. (d) Drain current (I_d)–drain voltage (V_d) characteristics for two different 10–20 nm as-deposited Si NC FETs.[122]

4.3. Photocatalysts

Heterogeneous nanocatalysis is a fascinating field in nanotechnology. Although numerous kinds of metal oxide and sulfides have been investigated and improved by changing the chemical composition, surface fabrication and energy gap,[123,124] silicon nanostructures, such as H-terminated nanowires, porous silicon nanowires and silicon nanoparticles also win a space in this domain for themselves.[125–127] In this respect, our group has already successfully prepared silicon QDs with dimensions of 1–4 nm by high energy ball milling (Fig. 11(a)) and concluded that the pure Si NCs without any capping of molecules on their surfaces exhibit excellent rates for conversion of carbon dioxide into aldehyde. By quantifying the concentration of the resulting formaldehyde by adding Nash reagent to samples and monitoring its maximum absorbance at 412 nm under three contrast tests (Fig. 11(b)), we found that the exposed Si QDs can serve as efficient photocatalysts for effective recombination between electrons/holes induced by photons and CO_2/H_2O, respectively.[128]

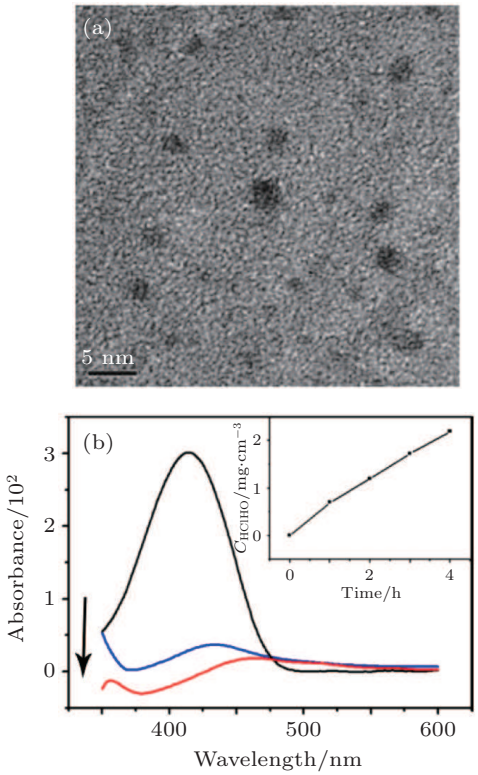


Fig. 11. (color online) (a) TEM image of Si NCs produced by HEMB for 3-h illumination. (b) UV–visible spectra of the reaction solution (after 2-h illumination) treated with Nash reagent for the determination of formaldehyde. As the arrow indicates, from the top to bottom, the line represents obtained UV–visible data in the presence of unmodified Si NCs with illumination, in the absence of illumination and in the absence of unmodified Si NCs, respectively. Inset: the concentration of formaldehyde as a function of reaction time.[128]

By following an electrochemical etching recipe, 1–2 nm and 3–4 nm Si QDs were prepared respectively by Kang *et al*.[127] Here, they demonstrated that CO_2 reduction and dye (methyl red) degradation can be effectively proceeded by utilizing 1–2 nm Si QDs serving as an excellent photocatalyst, whereas 3–4 nm QDs are for the selective oxidation of benzene instead of the reduction of CO_2/CO_3^{2-} or the degradation of methyl red (Fig. 12). The striking difference between them may be due to the larger electron/hole pair energy of 1–2 nm Si QDs than that of 3–4 nm Si QDs which is responsible for its limited usage. Despite this, 3–4 nm Si QDs can potentially function as a photocatalyst for the hydroxylation of benzene by H_2O_2. In this process, the Si–SiO_x core–shell structure stemming from partially oxidized H-terminated Si QDs actually fulfilled its photocatalytic duty, on which H_2O_2 molecules were absorbed and decomposed into active oxygen species with oxene characteristics, which were electrophilic and prone to oxidize benzene rings into phenol and simultaneously the photoelectron reductive atmospheric protected it from further oxidizing which might lead to high selectivity of phenol formation.[127]

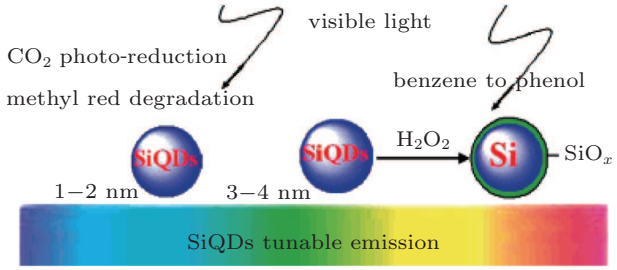


Fig. 12. (color online) Schemetics for Si QDs of different diameters from different reactions.[127]

5. Summary and prospects

The strategies to synthesize silicon nanoparticles, utilizing different apparatus and chemical compositions, have advanced significantly during the past 50 years. There are numerous synthesis routes for silicon nanocrystals featuring distinctive characteristics. Physical processes generally produce limited yields of pure products but can get rid of contaminants originating from byproducts. While chemical routes tend to scale up the yields and complete further functionalization synchronously, they are plagued by impure products. Efficient modification methods based on different exterior bonds such as Si–H, Si–Si, Si–C, Si–OH can significantly lead to a better understanding of its essential optical and electric properties. This article also discusses a range of applications which are rapidly developing and have extended to broad fields. Among these, we focus on exploring their potential in energy and biomedical applications, and as nanocatalysts—all show a promising future.

Despite the fact that there are already myriad researches on Si QDs, the natures of certain properties are still unclear. So, more investigations are necessary to confirm whether there are any other theories except quantum confinement and oxide-related defects, which can grasp the comprehensive principles to explain some amazing phenomena such as PL quenching when sensing some chemical molecules. Other potential avenues of research may include improvements in synthetic

strategies to produce stable silicon colloids dispersed in a wide range of solvents instead of the given one, and to reliably fabricate controlled particles with an appropriate size and biochemical functional groups for more extensive applications. There is no doubt that the attention paid to the field of Si NPs will increase—more creative research results are expected to be presented—and this material will have an immeasurable influence on the future society.

References

[1] Cullis A G and Canham L T 1991 *Nature* **353** 26
[2] Fujioka K, Hiruoka M, Sato K, Manabe N, Miyasaka R, Hanada S, Hoshino A, Tilley R D, Manome Y and Hirakuri K 2008 *Nanotecnology* **19** 415102
[3] Moore D, Krishnamurthy S, Chao Y, Wang Q, Brabazon D and McNally P J 2011 *Phys. Status Solidi A* **208** 604
[4] Weis S, Körmer R, Jank M P M, Lemberger M, Otto M, Ryssel H, Peukert W and Frey L 2011 *Small* **7** 2853
[5] Shirahata N 2011 *Phys. Chem. Chem. Phys* **13** 7284
[6] Gao X H, Cui Y Y, Levenson R M, Chung L W K and Nie S M 2004 *Nat. Biotechnol.* **22** 969
[7] Astruc D, Lu F and Aranzaes J R 2005 *Angew. Chem. Int. Ed.* **44** 7852
[8] Schuppler S, Friedman S L, Marcus M A, Adler D L, Xie Y H, Ross F M, Chabal Y J, Harris T D, Brus L E, Brown W L, Chaban E E, Szajowski P F, Christman S B and Citrin P H 1995 *Phys. Rev. B* **52** 4910
[9] Saar A 2009 *J. Nanophoton.* **3** 032501
[10] Zou J, Sanelle P, Pettigrew K A and Kauzlarich S M 2006 *J. Cluster Sci.* **17** 565
[11] Talapin D V, Lee J S, Kovalenko M V and Shevchenko E V 2009 *Chem. Rev.* **110** 389
[12] Lewinski N, Colvin V and Drezek R 2008 *Small* **4** 26
[13] Powers D E, Hansen S G, Geusic M E, Puiu A C, Hopkins J B, Dietz T G, Duncan M A, Langridge-Smith P R R and Smalley R E 1982 *J. Phys. Chem.* **86** 2556
[14] Hopkins J B, Langridge-Smith P R R, Morse M D and Smalley R E 1983 *J. Chem. Phys.* **78** 1627
[15] Yoshida T, Takeyama S, Yamada Y and Mutoh K 1996 *Appl. Phys. Lett.* **68** 1772
[16] Wang Y L, Xu W, Zhou Y, Chu L Z and Fu G S 2007 *Laser and Particle Beams* **25** 9
[17] Kuzmin P G, Shafeev G A, Bukin V V, Garnov S V, Farcau C, Carles R, Fontrose B W, Guieu V and Viau G 2010 *J. Phys. Chem. C* **114** 15266
[18] Intartaglia R, Bagga K, Scotto M, Diaspro A and Brandi F 2012 *Opt. Mater. Express* **2** 510
[19] Abderrafi K, Calzada R G, Gongalsky M B, Suárez I, Abarques R, Chirvony V S, Timoshenko V Y, Ibánez R and Martínez-Pastor J P 2011 *J. Phys. Chem. C* **115** 5147
[20] Intartaglia R, Barchanski A, Bagga K, Genovese A, Das G, Wagener P, Fabrizio E D, Diaspro A, Brandi F and Barcikowski S 2012 *Nanoscale* **4** 1271
[21] Petersen S and Barcikowski S 2009 *Adv. Funct. Mater.* **19** 1167
[22] Ho P, Coltrin M E and Breiland W G 1994 *J. Phys. Chem.* **98** 10138
[23] Swihart M T and Girshick S L 1999 *J. Phys. Chem. B* **103** 64
[24] English D S, Pell L E, Yu Z H, Barbara P F and Korgel B A 2002 *Nano Lett.* **2** 681
[25] Shafeev G A, Freysz E and Bozon-Verduraz F 2004 *Appl. Phys. A* **78** 307
[26] Knipping J, Wiggers H, Rellinghaus B, Roth P, Konjhodzic D and Meier C 2004 *J. Nanosci. Nanotechnol.* **4** 1039
[27] He Y, Kang Z H, Li Q S, Tsang C H A, Fan C H and Lee S T 2009 *Angew. Chem.* **121** 134
[28] Panda A B, Glaspell G and El-Shall M S 2006 *J. Am. Chem. Soc.* **128** 2790
[29] He Y, Zhong Y L, Peng F, Wei X P, Su Y Y, Lu Y M, Su S, Gu W, Liao L S and Lee S T 2011 *J. Am. Chem. Soc.* **133** 14192
[30] Atkins T M, Thibert A, Larsen D S, Dey S, Browning N D and Kauzlarich S M 2011 *J. Am. Chem. Soc.* **133** 20664
[31] Lam C, Zhang Y F, Tang Y H, Lee C S, Bello I and Lee S T 2000 *J. Cryst. Growth* **220** 466
[32] Erogbogbo F, Yong K T, Hu R, Law W C, Ding H, Chang C W, Prasad P N and Swihart M T 2010 *ACS Nano* **4** 5131
[33] Ehbrecht M and Huisken F 1999 *Phys. Rev. B* **59** 2975
[34] Zhang X M, Neiner D, Wang S Z, Louie A Y and Kauzlarich S M 2007 *Nanotechnology* **18** 095601
[35] Li X G, He Y Q and Swihart M T 2004 *Langmuir* **20** 4720
[36] Li X G, He Y Q, Talukdar S S and Swihart M T 2003 *Langmuir* **19** 8490
[37] Huisken F, Ledoux G, Guillois O and Reynaud C 2002 *Adv. Mater.* **14** 1861
[38] Heath J R 1992 *Science* **258** 1131
[39] Baldwin R K, Pettigrew K A, Ratai E, Augustine M P and Kauzlarich S M 2002 *Chem. Commun.* **17** 1822
[40] Kornowski A, Giersig M, Vogel R, Chemseddine A and Weller H 1993 *Adv. Mater.* **5** 634
[41] Hapala P, Kůsová K, Pelant I and Jelínek P 2013 *Phys. Rev. B* **87** 195420
[42] Sudeep P K, Page Z and Emrick T 2008 *Chem. Commun.* **46** 6126
[43] Bley R A and Kauzlarich S M 1996 *J. Am. Chem. Soc.* **118** 12461
[44] Wilcoxon J P, Samara G A and Provencio P N 1999 *Phys. Rev. B* **60** 2704
[45] Wang J and Sun S Q 2011 *Sci. Sin. Phys. Mech. Astron.* **41** 1041 (in Chinese)
[46] Tilley R D and Yamamoto K 2006 *Adv. Mater.* **18** 2053
[47] Wang J, Sun S Q, Peng F, Cao L X and Sun L F 2011 *Chem. Commun.* **17** 4941
[48] Zhang X M, Neiner D, Wang S Z, Louie A Y and Kauzlarich S M 2007 *Nanotechnology* **18** 095601
[49] McMillan P F, Gryko J, Bull C, Arledge R, Kenyon A J and Cressey B A 2005 *J. Solid State Chem.* **178** 937
[50] Zhang X M, Brynda M, Britt R D, Carroll E C, Larsen D S, Louie A Y and Kauzlarich S M 2007 *J. Am. Chem. Soc.* **129** 10668
[51] Ahire J H, Wang Q, Coxon P R, Malhotra G, Brydson R, Chen R J and Chao Y M 2012 *ACS Appl. Mater. Interfaces* **4** 3285
[52] Wang J, Liu Y X, Peng F, Chen C Y, He Y H, Ma H, Cao L X and Sun S Q 2012 *Small* **8** 2430
[53] Wang Q, Bao Y P, Zhang X H, Coxon P R, Jayasooriya U A and Chao Y M 2012 *Adv. Healthc. Mater.* **1** 189
[54] Coxon P R, Wang Q and Chao Y M 2011 *J. Phys. D: Appl. Phys.* **44** 495301
[55] Alsharif N H, Berger C E M, Varanasi S S, Chao Y M, Horrocks B R and Datta H K 2009 *Small* **5** 221
[56] Bley R A, Kauzlarich S M, Davis J E and Lee H W 1996 *Chem. Mater.* **8** 1881
[57] Sailor M J and Wu E C 2009 *Adv. Funct. Mater.* **19** 3195
[58] Wilson W L, Szajowski P F and Brus L E 1993 *Science* **262** 1242
[59] Zhu X P, Yukawa T, Kishi T, Hirai M, Suematsu H, Jiang W H and Yatsui K 2005 *J. Nanopart. Res.* **7** 669
[60] Sato S and Swihart M T 2006 *Chem. Mater.* **18** 4083
[61] Duke C B 1996 *Chem. Rev.* **96** 1237
[62] Bent S F 2002 *Surf. Sci.* **500** 879
[63] Waltenburg H N and Yates J T 1995 *Chem. Rev.* **95** 1589
[64] Ruizendaal L, Pujari S P, Gevaerts V, Paulusse J M and Zuilhof H 2011 *J. Asian Chem.* **6** 2776
[65] Shiohara A, Hanada S, Prabakar S, Fujioka K, Lim T H, Yamamoto K, Northcote P T and Tilley R D 2009 *J. Am. Chem. Soc.* **132** 248
[66] Tilley R D, Warner J H, Yamamoto K, Matsui I and Fujimori H 2005 *Chem. Commun.* **14** 1833
[67] Kang Z H, Liu Y, Tsang C H A, Ma D D D, Fan X, Wong N B and Lee S T 2009 *Adv. Mater.* **21** 661
[68] RossoVasic M, Spruijt E, Lagen B V, Cola L D and Zuilhof H 2008 *Small* **4** 1835
[69] Dinh L N, Chase L L, Balooch M, Siekhaus W J and Wooten F 1996 *Phys. Rev. B* **54** 5029
[70] Li Z F and Ruckenstein E 2004 *Nano Lett.* **4** 1463
[71] Secret E, Maynadier M, Gallud A, Gary-Bobo M, Chaix A, Belamie E, Maillard P, Sailor M J, Garcia M, Durand J O and Cunin F 2013 *Chem. Commun.* **49** 4202
[72] Gelloz B and Koshida N 2009 *Appl. Phys. Lett.* **94** 201903
[73] Zhong Y L, Peng F, Wei X P, Zhou Y F, Wang J, Jiang X X, Su Y Y, Su S, Lee S T and He Y 2012 *Angew. Chem. Int. Ed.* **51** 8485

[74] Shiohara A, Prabakar S, Faramus A, Hsu C Y, Lai P S, Northcote P T and Tilley R D 2011 *Nanoscale* **3** 3364
[75] Delerue C, Allan G and Lannoo M 1993 *Phys. Rev. B* **48** 11024
[76] Cho S T, Tsai J H and Sheu B C 1998 *J. Appl. Phys.* **83** 10
[77] Iacona F, Franzo G and Spinella C 2000 *J. Appl. Phys.* **87** 1295
[78] Hill N A and Whaley K B 1995 *Phys. Rev. Lett.* **75** 1130
[79] Ledoux G, Gong J, Huisken F, Guillois O and Reynaud C 2002 *Appl. Phys. Lett.* **80** 4834
[80] Trwoga P F, Kenyon A J and Pitt C W 1998 *J. Appl. Phys.* **83** 3789
[81] Meier C, Gondorf A, Lüttjohann S, Lorke A and Wiggers H 2007 *J. Appl. Phys.* **101** 103112
[82] Mangolini L, Thimesen E and Kortshagen U 2005 *Nano Lett.* **5** 655
[83] Chao Y, Krishnamurthy S, Montalti M, Lie L H, Houlton A, Horrocks B R, Kjeldgaard L, Dhanak V R, Hunt M R C and Siller L 2005 *J. Appl. Phys.* **98** 044316
[84] Anthony R and Kortshagen U 2009 *Phys. Rev. B* **80** 115407
[85] Ledoux G, Gong J, Huisken F, Guillois O and Reynaud C 2002 *Appl. Phys. Lett.* **80** 4834
[86] Pi X D, Liptak R W, Campbell S A and Kortshagen U 2007 *Appl. Phys. Lett.* **91** 083112
[87] Hua F J, Erogbogbo F, Swihart M T and Ruckenstein E 2006 *Langmuir* **22** 4363
[88] Dasog M, Yang Z Y, Regli S, Atkins T M, Faramus A, Singh M P, Muthuswamy E, Kauzlarich S M, Tilley R D and Veinot J G C 2013 *ACS Nano* **7** 2676
[89] Nekrashevich S S and Gritsenko V A 2011 *J. Appl. Phys.* **110** 114103
[90] Yang S K, Li W Z, Cao B Q, Zeng H B and Cai W P 2011 *J. Phys. Chem. C* **115** 21056
[91] Zou J, Baldwin R K, Pettigrew K A and Kauzlarich S M 2004 *Nano Lett.* **4** 1181
[92] Ashby S P, Thomas J A, Coxon P R, Bilton M, Brydson R, Pennycook T J and Chao Y M 2013 *J. Nanopart. Res.* **5** 1
[93] Li Q, He Y, Chang J, Wang L, Chen H Z, Tan Y W, Wang H and Shao Z Z 2013 *J. Am. Chem. Soc.* **135** 14924
[94] Mertens H, Biteen J S, Atwater H A and Polman A 2006 *Nano Lett.* **6** 2622
[95] Singh M P, Atkins T M, Muthuswamy E, Kamali S, Tu C Q, Louie A Y and Kauzlarich S M 2012 *ACS Nano* **6** 5596
[96] Sato K, Yokosuka S, Takigami Y, Hirakur K, Fujioka K, Manome Y, Sukegawa H, Iwai H and Fukata N 2011 *J. Am. Chem. Soc.* **133** 18626
[97] Fu Y H, Kuznetsov A I, Miroshnichenko A E, Yu Y F and Luk'yanchuk B 2013 *Nat. Commun.* **4** 1527
[98] Van Buuren T, Dinh L N, Chase L L, Siekhaus W J and Terminello L J 1998 *Phys. Rev. Lett.* **80** 3803
[99] Yang P, Gwilliam R M, Crowe I F, Papachristodoulou N, Halsall M P, Hylton N P, Hulko O, Knights A P, Shah M and Kenyon A J 2013 *Nucl. Instrum. Methods Phys. Res. Sect. B* **307** 456
[100] Hapala P, Kůsová K, Pelant I and Jelínek P 2013 *Phys. Rev. B* **87** 195420
[101] Stegner A R, Pereira R N, Klein K, Lechner R, Dietmueller R, Brandt M S, Stutzmann M and Wiggers H 2008 *Phys. Res. Lett.* **100** 026803
[102] Al Ahmed S R and Ismail A B M 2013 *Int. J. Eng. Res. Technol.* **2** 3170
[103] Manousiadis P, Gardelis S and Nassiopoulou A G 2013 *J. Appl. Phys.* **113** 043703
[104] Ramos E, Monroy B M, Alonso J C, Sansores L E, Salcedo R and Martínez A 2012 *J. Phys. Chem. C* **116** 3988
[105] Nelles J, Sendor D, Petrat F M and Simon U 2010 *J. Nanopart. Res.* **12** 1367
[106] Niesar S, Pereira R N, Stegner A R, Erhard N, Hoeb M, Baumer A, Wiggers H, Brandt M S and Stutzmann M 2012 *Adv. Funct. Mater.* **22** 1190
[107] Kim S K, Cho C H, Kim B H, Park S J and Lee J W 2009 *Appl. Phys. Lett.* **95** 143120
[108] Cheng K Y, Anthony R, Kortshagen U R and Holmes R J 2011 *Nano Lett.* **11** 1952
[109] Puzzo D P, Henderson E J, Helander M G, Wang Z B, Ozin G A and Lu Z H 2011 *Nano Lett.* **11** 1585
[110] Maier-Flaig F, Rinck J, Stephan M, Bocksrocker T, Bruns M, Kübel C, Powell A K, Ozin G A and Lemmer U 2013 *Nano Lett.* **13** 475
[111] Conibeer G, Green M, Cho E C, König D, Cho Y H, Fangsuwannarak T, Scardera G, Pink E, Huang Y D, Puzzer T, Huang S J, Song D Y, Flynn C, Park S, Hao X J and Mansfield D 2008 *Thin Solid Films* **516** 6748
[112] Conibeer G, Green M, Corkish R, Cho Y, Cho E C, Jiang C W, Fangsuwannarak T, Pink E, Huang Y D, Puzzer T, Trupke T, Richards B, Shalav A and Lin K L 2006 *Thin Solid Films* **511** 654
[113] Cho E C, Park S, Hao X J, Song D Y, Conibeer G, Park S C and Green M A 2008 *Nanotechnology* **19** 245201
[114] Zhou S, Liu X H and Wang D W 2010 *Nano Lett.* **10** 860
[115] Chan C K, Patel R N, O'Connell M J, Korgel B A and Cui Y 2010 *ACS Nano* **4** 1443
[116] Ge M Y, Rong J P, Fang X and Zhou C W 2012 *Nano Lett.* **12** 2318
[117] Yao Y, McDowell M T, Ryu I, Wu H, Liu N, Hu L B, Nix W D and Cui Y 2011 *Nano Lett.* **11** 2949
[118] Guo J C, Yang Z C and Archer L A 2013 *J. Mater. Chem. A* **1** 5709
[119] Ge M Y, Rong J P, Fang X, Zhang A Y, Lu Y H and Zhou C W 2013 *Nano Res.* **3** 174
[120] Takeda Y and Motohiro T 2011 *Sol. Energy Mater. Sol. Cells* **95** 2638
[121] Ridley B A, Nivi B and Jacobson J M 1999 *Science* **286** 746
[122] Holman Z C, Liu C Y and Kortshagen U R 2010 *Nano Lett.* **10** 2661
[123] Wang B, Leung M K H, Lu X Y and Chen S Y 2013 *Appl. Energy* **112** 1190
[124] Mase A, Sugita T, Mori M, Iwamoto S, Tokutome T, Katayama K and Itabashi H 2013 *Chem. Eng. J.* **225** 440
[125] Qu Y Q, Zhong X, Li Y J, Liao L, Huang Y and Duan X F 2010 *J. Mater. Chem.* **20** 3590
[126] Shao M W, Cheng L, Zhang X H, Ma D D D and Lee S T 2009 *J. Am. Chem. Soc.* **131** 17738
[127] Kang Z H, Tsang C H A, Wong N B, Zhang Z D and Lee S T 2007 *J. Am. Chem. Soc.* **129** 12090
[128] Peng F, Wang J, Ge G L, He T, Cao L X, He Y H, Ma H and Sun S Q 2013 *Mater. Lett.* **92** 65